Biosensors and Bioelectronics 156 (2020) 112133

Contents lists available at ScienceDirect

Biosensors and Bioelectronics

journal homepage: http://www.elsevier.com/locate/bios

A wearable lab-on-a-patch platform with stretchable nanostructured biosensor for non-invasive immunodetection of biomarker in sweat

Han-Byeol Lee [a], Montri Meeseepong [b], Tran Quang Trung [a], Bo-Yeong Kim [b], Nae-Eung Lee [a,b,c,d,e,*]

[a] School of Advanced Materials Science & Engineering, Sungkyunkwan University, 2066 Seobu-ro, Jangan-gu, Suwon-si, Gyunggi-do, 16419, South Korea
[b] SKKU Advanced Institute of Nano Technology (SAINT), Sungkyunkwan University, 2066 Seobu-ro, Jangan-gu, Suwon-si, Gyunggi-do, 16419, South Korea
[c] Samsung Advanced Institute for Health Sciences and Technology (SAIHST), Sungkyunkwan University, 2066 Seobu-ro, Jangan-gu, Suwon-si, Gyunggi-do, 16419, South Korea
[d] Institute of Quantum Biophysics (IQB), Sungkyunkwan University, 2066 Seobu-ro, Jangan-gu, Suwon-si, Gyunggi-do, 16419, South Korea
[e] Biomedical Institute for Convergence at SKKU (BICS) Sungkyunkwan University, 2066 Seobu-ro, Jangan-gu, Suwon-si, Gyunggi-do, 16419, South Korea

ARTICLE INFO

Keywords:
Stretchable biosensor
Microfluidics
Immunodetection
Wearable device
3D nanostructured impedimetric biosensor

ABSTRACT

Conformable, wearable biosensor-integrated systems are a promising approach to non-invasive and quantitative on-body detection of biomarkers in body fluids. However, realizing such a system has been slowed by the difficulty of fabricating a soft affinity-based biosensor patch capable of precise on-body fluid handling with minimal wearer intervention and a simple measurement protocol. Herein, we demonstrate a conformable, wearable lab-on-a-patch (LOP) platform composed of a stretchable, label-free, impedimetric biosensor and a stretchable microfluidic device for on-body detection of the hormone biomarker, cortisol. The all-in-one, stretchable microfluidic device can precisely collect and deliver sweat for cortisol quantitation and offers one-touch operation of reagent delivery for simultaneous electrochemical signal generation and washing. Three-dimensional nanostructuring of the Au working electrode enables the high sensitivity required to detect the pM-levels of cortisol in sweat. Our integrated LOP detected sweat cortisol quantitatively and accurately during exercise. This LOP will open a new horizon for non-invasive, highly sensitive, and quantitative on-body immunodetection for wearable personal diagnostics.

1. Introduction

Personal diagnostics and health monitoring are expected to play an important role in the emerging areas of personalized and preventive healthcare. Wearable biosensor-integrated diagnostic devices are a promising approach because of their user convenience; they require no separate off-body sample handling and offer high connectivity and ease of access (Andreu-Perez et al., 2015; Bariya et al., 2018; Heikenfeld et al., 2018; Imani et al., 2016; Kim et al., 2019b; Lee et al., 2019; Ray et al., 2019; Trung and Lee, 2016; Windmiller and Wang, 2013). Soft, skin-mountable biosensor patches are of particular interest for non-invasive or minimally invasive detection of biomarkers from body fluids such as sweat, interstitial fluids, or wound exudate (Bandodkar et al., 2019; Guinovart et al., 2014; Kassal et al., 2015; Matzeu et al., 2015; Salvo et al., 2015; Xu et al., 2019b; Zhao et al., 2019). The most recent research has been limited to continuous monitoring of metabolites such as glucose and lactate in body fluids using flexible (Emaminejad et al., 2017; Gao et al., 2016; Gao et al., 2019; He et al., 2019; Jia et al., 2013; Lee et al., 2016a) or stretchable biosensor patches (Bae et al., 2019; Choi et al., 2018; Huang et al., 2014; Kim et al., 2019a; Kim et al., 2018; Koh et al., 2016; Martín et al., 2017; Reeder et al., 2019; Toi et al., 2019; Xu et al., 2019a). Future personal diagnostics and health monitoring, however, will require soft, skin-mountable biosensor patches that can detect proteins or small molecules using an affinity-based biosensing scheme (Bandodkar et al., 2016; Bandodkar and Wang, 2014; Bariya et al., 2018; Heikenfeld et al., 2018; Kim et al., 2019b; Someya and Amagai, 2019; Windmiller and Wang, 2013). Currently, the development of such immunosensor patches has been slowed by many challenges in realizing precise on-body handling of body fluid samples and reagents, good conformability for convenient

* Corresponding author. School of Advanced Materials Science & Engineering, Sungkyunkwan University, 2066 Seobu-ro, Jangan-gu, Suwon-si, Gyunggi-do, 16419, South Korea.
E-mail address: nelee@skku.edu (N.-E. Lee).

https://doi.org/10.1016/j.bios.2020.112133
Received 5 December 2019; Received in revised form 18 February 2020; Accepted 2 March 2020
Available online 6 March 2020

on-body operation, a low limit of detection (LOD) and high accuracy, and a simple detection protocol with seamless integration from sampling to detection.

The concept of soft, conformable, skin-mountable biosensor patches for wearable on-body detection of biomarkers is of great interest because they would be much more convenient for users than lab-based immunoassays or in-hospital point-of-care testing (POCT), which require many off-body sample handling steps and user expertise in sample analysis. However, many obstacles block the way to high-performance quantitative detection of proteins or small molecules using affinity-based immunosensing in soft, skin-mountable biosensor patches (Daniels and Pourmand, 2007; Meng et al., 2019): on-body sampling of body fluids, transport control of the collected sample and reagent fluids without the use of electrically powered pumps, quantitative and accurate measurement of low-concentration target biomolecules in body fluids other than blood (pM level or less), securing and maintaining skin contact during bodily motion, and adequately simplifying the measurement protocol (labeling, washing, reagent delivery, etc.) (Corrie et al., 2015; Han et al., 2013; Kokkinos et al., 2016; Tomazelli Coltro et al., 2014). Many existing immunodetection procedures use labeling, in which an enzyme, fluorescent tag, or redox couple is attached to a detection probe to generate a detection signal, but those techniques are time-consuming, require multi-step operations, and cause inconvenience to the wearer (Joung et al., 2019; Kallempudi et al., 2012). Unlike the separate steps typically used in conventional POCT, collecting a sample, handling the collected sample, and measuring the marker of interest (all by expert operators), a wearable biosensor patch requires a seamlessly integrated protocol that extends from precise sample collection to reagent delivery and measurement with minimal user intervention.

Herein, we demonstrate a new, fully stretchable, wearable, lab-on-a-patch (LOP) platform that integrates a stretchable impedimetric biosensor with a stretchable passive microfluidic device for non-invasive, wearable immunodetection of the hormone biomarker cortisol in sweat. Cortisol, a notable part of the human stress response and regulator of the immune system, is generated by the adrenal glands. The cortisol level in sweat is known to correlate well with the level in blood, and the cortisol in sweat exists in a free form, making non-invasive detection of cortisol in sweat using a wearable biosensor a feasible possibility (Steckl and Ray, 2018). Daily measurement of cortisol using a disposable LOP can provide useful information since excessive or deficiency of cortisol level gives the alarm of health such as Cushing's syndrome or Addison's disease. To address the critical issues of wearable immunodetection of cortisol, we developed a stretchable, all-in-one, microfluidic device that can autonomously and precisely collect and deliver a fixed volume of sweat for quantitative measurement and a one-touch finger operation to deliver reagent from a reservoir for simultaneous signal generation and washing (Fig. 1a) We integrated our LOP with a stretchable, highly sensitive, and label-free impedimetric biosensor that uses a working electrode of three-dimensional (3D) nanostructured Au for signal enhancement and has a faradaic signal readout with a redox mediator. Using an antibody (Ab) as a probe biomolecule, our biosensor stably detected cortisol levels from 1 pg/ml to 1 μg/ml, even under an applied 30% strain. The integrated microfluidic-device and electrochemical biosensor patch successfully performed precise, on-body sweat sampling and cortisol measurement down to the pM concentration range. The wearable biosensor patch quantitatively detected sweat cortisol during exercise with a high correlation (relative difference of ~14.7%) to the standard enzyme-linked immunosorbent assay (ELISA) assay used with conventionally collected sweat samples. Our integrated LOP has great potential as a wearable immunodetection platform for personal diagnostics and health monitoring.

2. Materials and methods

Reagent, materials, microfluidic design, fabrication methods, and measurement protocol can be found in the Supplementary Information.

3. Results and discussion

3.1. Design concept for a conformable, integrated microfluidics and biosensor patch

To realize a soft, conformable, wearable biosensor patch that can provide microfluidic fluid control, we designed a new microfluidic device for simple, passive, and precise sample handling without electrical power (left panel, Fig. 1b) and the patch integrates a stretchable impedimetric biosensor and the microfluidic device (right panel, Fig. 1b). The microfluidic device is made of two layers of PDMS cast from 3D-printed resin molds. The fluid passage layer (FPL) and fluid connection layer (FCL) are formed into a sweat inlet chamber (I), sensing chamber (S), waste disposal chamber (D), reagent (redox mediator) reservoir (R), and microfluidic channels connecting them with one another (Fig. 1c).

The passive microfluidic device is operated in the following sequence: sweat is passively absorbed through the inlet to the I and delivered to the S where it is incubated for about 15 min without the introduction of new sweat, precisely metering the sweat volume for quantitative detection. The reagent is injected from the R into the S when the user presses a button, which begins a sequence of redox mediator delivery, electrochemical signal measurement, and washing (Fig. S1). This passive microfluidic device is independent of any need for an external force, such as an electrically driven pump (Dastider et al., 2013; Oh et al., 2012), pressure from a sweat gland (Choi et al., 2018; Glennon et al., 2016; Imani et al., 2016; Koh et al., 2016), or inserted capillary materials such as a fabric (Jeerapan et al., 2016; Kassal et al., 2015; Panneer Selvam et al., 2016; Zamora et al., 2018), fiber (Bae et al., 2019; Tamayol et al., 2016; Zhong et al., 2014), or absorption pad (Alizadeh et al., 2018; Xu et al., 2019a). It is an all-in-one system that performs sampling, metering, reagent delivery, and washing to an integrated faradaic impedimetric biosensor for convenient on-body immunodetection.

3.2. Design and demonstration of passive microfluidic device for sample handling

Our passive microfluidic device uses several key innovations: 1) the I and S have hydrophilic surfaces to sustain autonomous sweat flow for a long time; 2) the button that users push on the R is tapered to prevent backflow of the reagent during operation; 3) fine zig-zag-patterned capillaries on the FPL portion allow the S to collect sweat uniformly and fill entirely, and 4) our unique arched flap valve, burst valve, and check valve in the channels between the I–S, S-D, and S-R, respectively, hold the sweat in the S during incubation for Ab-cortisol binding and then allow the reacted sweat to burst out as the reagent in the R is injected into the S (Fig. 1d).

To ensure that sweat passively flows from skin along the microfluidic channels, the I, S, and microfluidic channel between them received a surface treatment of covalent bonding with polyvinylpyrrolidone (PVP), a polar molecule, for long-term hydrophilicity. PVP also has an anti-biofouling characteristic and provides long-term, sustainable hydrophilicity of PDMS (Gokaltun et al., 2017). Immediately after treatment, the contact angles of the PDMS substrates treated by O_2 plasma and PVP were both about 5°. However, the contact angle of the PDMS treated with O_2 plasma increased over time, reaching 80° after one day, indicating that the hydrophilicity created by the O_2 plasma treatment cannot be maintained. On the other hand, the contact angle of the PDMS substrate treated with PVP did not change significantly even after 6 days, as shown in Fig. 1e and more detailed results are provided in Fig. S2.

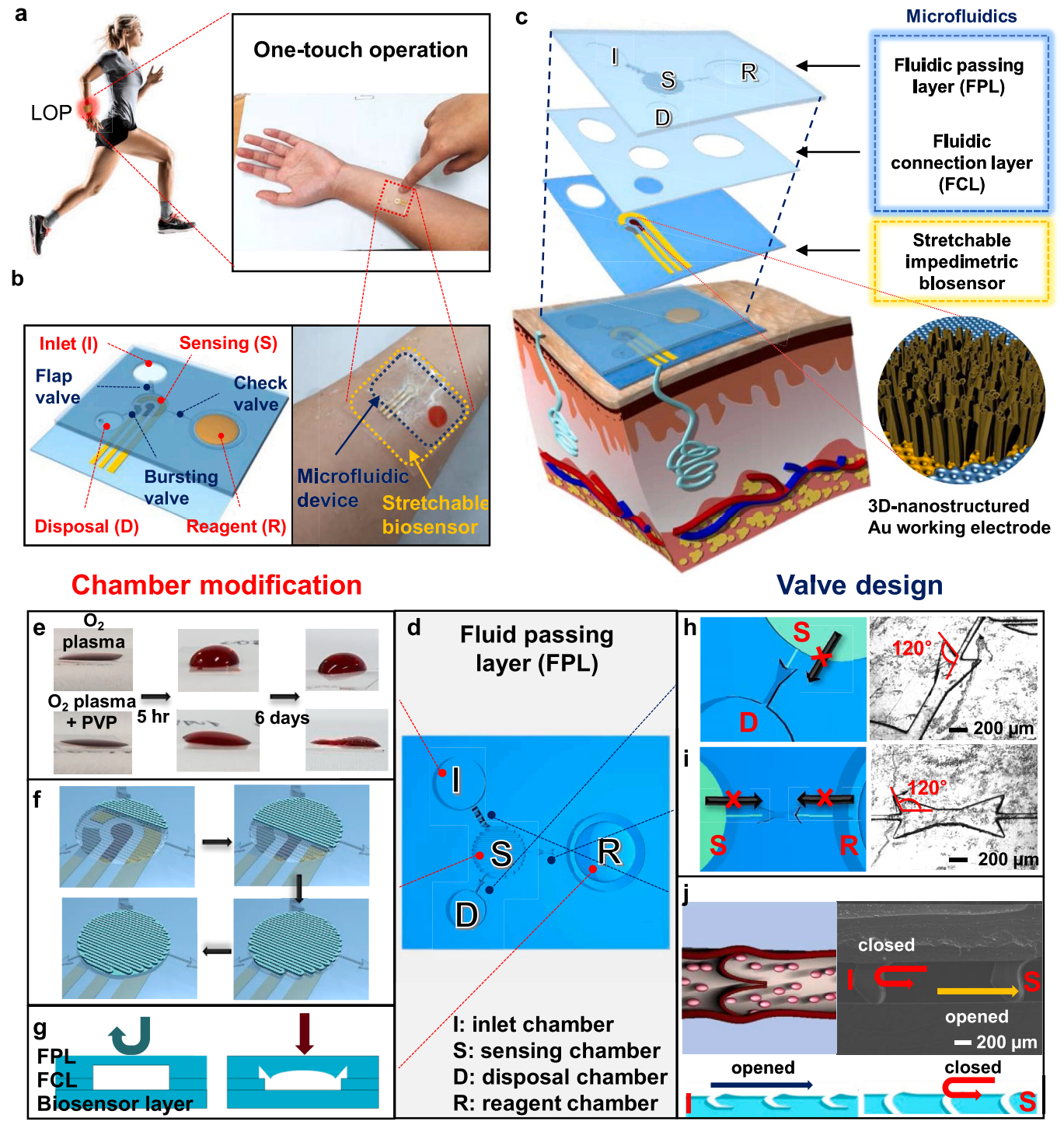

(caption on next page)

Fig. 1. LOP with microfluidic and electrochemical sensing components for wearable POCT. (a) Schematic diagram of the LOP platform for wearable biomarker detection. A microfluidic device integrated with an electrochemical biosensor in a patch is attached to human skin. The microfluidic device collects a sweat sample, transports the sample to a sensing chamber containing a stretchable impedimetric immunosensor, delivers reagent (redox mediator) and washes the sensing chamber simultaneously, and disposes of the waste. A measurement protocol based on the faradaic EIS technique reduces the need for user intervention to a one-touch finger push to deliver the mediator for signal transduction. **(b)** A schematic view of the LOP (left) and a picture of the LOP attached to a forearm (right). The main components are a stretchable microfluidic device to handle the sample and reagent and a stretchable impedimetric biosensor with a Au 3D-nanostructured working electrode. The microfluidic device contains four chambers, the sweat inlet (I), sensing (S), disposal (D), and reagent (R) chambers, and three valves in the channels between the chambers specifically designed to control the fluid transport precisely. **(c)** An exploded view of the LOP platform. The top layer is the fluidic passing layer (FPL) with the chambers and channels. The middle layer is the fluidic connection layer (FCL) that connects the chambers to the skin on I in FPL and the sensor device region on the bottom layer containing stretchable impedimetric immunosensor with 3D-nanostructured Au working electrode fabricated on a mogul-patterned substrate. **(d)** Top-view image of the FPL: sweat inlet (I), sensing chamber (S), disposal chamber (D), reagent chamber (R), and connecting channels. **(e)** Side-view picture of PBS 1X solution dropped onto the oxygen plasma–treated PDMS and oxygen plasma–treated PDMS + PVP. This picture was taken with a smartphone camera. **(f)** Sequence of the fluid flow through the zig-zag patterned capillaries in the S that allow the fluid to fill the S completely. **(g)** Cross-sectional view of the push button on the R. Whereas the rectangular button returned to the initial state after being pushed (left), the taper-shaped button is fitted into a hole in the FCL and remains stuck at the bottom (right). **(h)** Bursting valve between the S and the D (left). Image of the bursting valve with the angle of the arrow at 120° (right). **(i)** Check valve between the S and R (left). Image of the check valve with the angle of the arrow at 120° (right). **(j)** Principle of venous valves in the human vascular system (top, left); cross-sectional FE-SEM image of the arched flap valve (top, right); operation of the arched flap valve, which opens as fluid flows from the I to the S and closes as fluid flows from the S to the I (bottom). **(k)** Demonstration of microfluidic device operation while it is attached to a forearm; artificial sweat with green dye was dropped on the skin, and the reagent chamber contained PBS 1X solution with red dye. (For interpretation of the references to colour in this figure legend, the reader is referred to the Web version of this article.)

When we made the I, S, and channels hydrophilic, we found that fluid passively flowed well from the I to the end of the channel but not into the S chamber, even though the S was hydrophilic. Therefore, we modified the inner side of the FPL composing the S with a fine, zig-zag pattern structure 200 μm wide to enhance the capillary effect (Stone et al., 2004). That treatment successfully allowed the fluid to fill up the entire S, as shown in Fig. 1f, Fig. S3, and **Supplementary Movie 1**

Supplementary video related to this article can be found at https://doi.org/10.1016/j.bios.2020.112133

The microfluidic device needs a reagent delivery component to replace the sweat in the S with reagent (redox mediator) solution for impedance measurement in the faradaic mode and to wash the S. The reagent solution is manually injected into the S with a one-touch mechanism that delivers the reagent from the R to the S. When the button on the FPL in the R was vertical, the pushing action delivered the solution into the S, but backflow occurred upon release (left panel of Fig. 1g, Figs. S4a–d, and **Supplementary Movie 2**). The negative pressure that drew the fluid flow backward was generated as the button recovered its original shape. The new tapered button design enables the reagent solution to flow from the R into the S without backflow because the inclined wall of the R in the FPL is pinched off in a hole in the FCL (right panel of Fig. 1g, Figs. S4e–f, and **Supplementary Movie 3)**.

Supplementary video related to this article can be found at https://doi.org/10.1016/j.bios.2020.112133

Realizing on-body label-free immunodetection requires control of the incubation time for target–probe (cortisol–cortisol Ab) binding and an ability to inject the redox mediator solution for the faradaic impedance reading. One salient feature in our microfluidic device is the design of three valves in the channels that control the flow precisely, as shown in Fig. 1h. First, a bursting valve is used in the channel between the S and the D to keep the sweat in the S during incubation. The sweat volume for measurement is autonomously metered because no more sweat can enter the S once it is full. The bursting valve bursts with the pressure generated during delivery of the reagent solution into the S after incubation. In our design, the maximum pressure difference that the valve can withstand, $(P_A - P_0)$, where P_A.and P_0 are the pressure inside and outside of liquid in the channel, respectively, was calculated as 1069.7 Pa for a channel width of 100 μm, a channel height of 250 μm , and a diverging angle in the channel (β) of $\frac{2}{3}\pi$. (more details are provided in Fig. S5 **and Supplementary Movies 4–6) (**Cho et al., 2007; Choi et al., 2017).

Supplementary video related to this article can be found at https://doi.org/10.1016/j.bios.2020.112133

The check valve between the S and the R is also used to control the incubation and prevent unintended fluid flow of the mediator solution in the R; it has the same bursting pressure as the bursting valve (Fig. 1i). By adopting bursting and check valves between the chambers, the target solution can be incubated in the S for a long time (~15 min) without a volume change or leakage of the collected sample, as shown in **Supplementary Movie 6**.

When the reagent solution is injected by pushing the R, the fluid flows toward the I rather than the D because of the surface hydrophilicity of the channel between the I and the S. Therefore, we designed and installed an arched flap valve inspired by the structure and function of venous valves in human veins to prevent the sweat in the S from flowing back toward the I during reagent injection into the S (Fig. 1j). Our arched flap valve arcs in the direction of the I (right panel in Fig. 2h), which acts like a venous valve (left panel in Fig. 2h) that is closed upon pushing the R and opened during the sampling stage (bottom panel in Fig. 2h) (Ramasamy, 2017). Because the R has a larger volume than the S, the reagent solution in the R can be effectively delivered to the S, replacing the reacted sweat in the S with the reagent and washing the S by pushing all the liquid toward the D.

To demonstrate the operation of our microfluidic device, we filled the R with a PBS 1X solution mixed with red dye, attached the device to a forearm, and dropped about 100 μL of artificial sweat mixed with green dye near it on the arm (Fig. 1k). The green artificial sweat flowed through the channel between the I and the S and entirely filled the S within 2 min, retaining the same volume (the burst valve in the channel between the S and the D did not burst) during the 15-min incubation. Then we pushed the top of the R, which injected the red PBS 1X solution into the S, displacing the green artificial sweat toward the D. Therefore, we deemed our passive microfluidic device ready for integration with a stretchable impedimetric biosensor to realize a skin-mountable biosensor patch (Fig. 1k and **Supplementary Movie 7**).

Supplementary video related to this article can be found at https://doi.org/10.1016/j.bios.2020.112133

3.3. Evaluation of stretchable impedimetric biosensor

The working electrode contains 3D-nanostructured Au to maximize the sensing signal by increasing the surface area, which increases the density of the Ab probes immobilized on it and minimizes its footprint, as shown in the cross-sectional and top-view field-emission scanning electron microscopy (FE-SEM) images (Fig. 2a). The increased surface area of this Au 3D-nanostructured working electrode can increase the current density while minimizing the footprint of the impedimetric biosensor (Chen et al., 2005, 2008; Haji-Hashemi et al., 2019; Pingarron et al., 2008). In the cyclic voltammetry (CV) curve, the cathodic current of the biosensor with the 3D-nanostructured Au was increased by a factor of 1.9 compared with that of a working electrode made of bare gold film (Fig. 2b). Also, the stretchable impedimetric biosensor shows

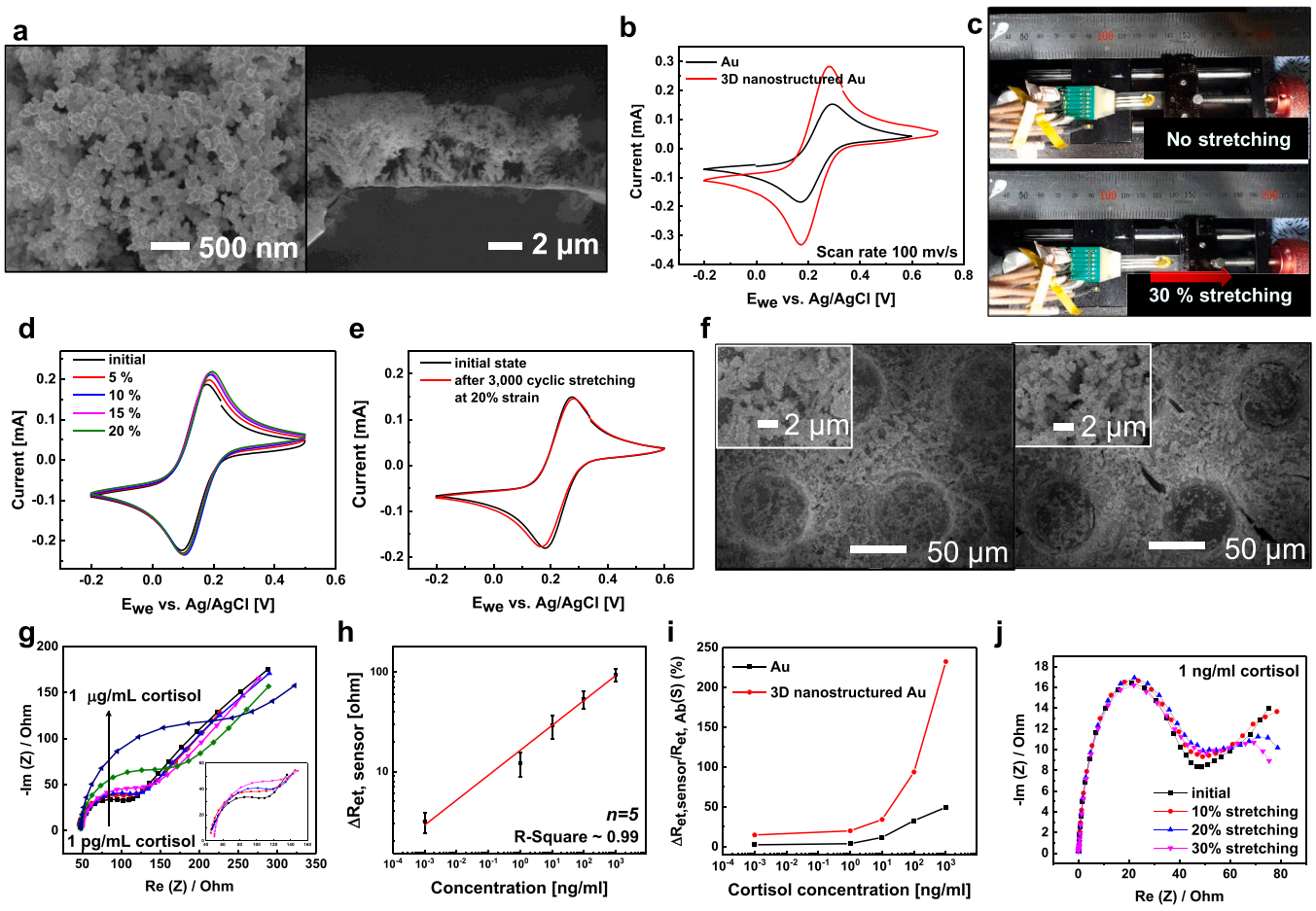

Fig. 2. Characterization of stretchable impedimetric biosensor with a Au 3D-nanostructured working electrode and performance of stretchable impedimetric biosensor. (a) Top-view (left panel) and cross-sectional (right panel) FE-SEM image of Au 3D-nanostructured working electrode. (b) Cyclic voltammetry (CV) curves for the biosensor with a Au film and the Au 3D-nanostructured working electrode in a 10 mM $K_3[Fe(CN)_6]$ and 1X PBS solution. **(c)** Pictures of the biosensor before (top panel) and after (bottom panel) being stretched (30%) by a customized stretching machine connected to a potentiostat. (d) CV curves for the stretchable biosensor under strains of 0–20% in a 10 mM $K_3[Fe(CN)_6]$ and 1X PBS solution. **(e)** CV curves for the stretchable impedimetric biosensor with the Au 3D-nanostructured working electrode before and after applying 3000 repetitions of cyclic stretching to 20% strain in a 10 mM $K_3[Fe(CN)_6]$ and 1X PBS solution. **(f)** Top-view FE-SEM image of the Au 3D-nanostructured working electrode before (left panel) and after (right panel) cyclic stretching. The insets show the magnified FE-SEM images of the Au 3D-nanostructrued working electrode. (g) Nyquist plots from the EIS measurements of the stretchable impedimetric biosensor at increasing cortisol (target) concentrations from 1 pg/ml to 1 μg/ml in artificial sweat. The inset show the Nyquist plots from the EIS measurement at increasing concentrations from 1 pg/ml to 10 ng/ml. (h) Calibration curve of the $\Delta R_{et,sensor}$ value as a function of cortisol concentration. (i) $\Delta R_{et,sensor}/R_{et,Ab}(\%)$ values from biosensors with Au film and Au 3D-nanostructured working electrodes at various cortisol concentrations. (j) Nyquist plot of the EIS measurements of the stretchable impedimetric biosensor under 10, 20, and 30% strain for a cortisol concentration of 1 ng/ml in a 10 mM $K_3[Fe(CN)_6]$ and 1X PBS solution.

good linearity with the scan rate, which indicates that it is suitable for electrochemical immunosensing (Fig. S6).

To evaluate the mechanical durability and stability of our stretchable impedimetric biosensor, we conducted CV testing in a 10 mM $K_3[Fe(CN)_6]$ in 1X PBS solution under static-stretched conditions from 0 to 20% strain and after 3000 cyclic stretches at 20% strain (Fig. 2c). The electrical signal of the stretchable impedimetric biosensor remained stable under stretching because the mogul-patterned substrate, which can effectively mitigate the stretching stress on the electrodes, enabling stable performance of the biosensor under mechanically stretched conditions (Lee et al., 2016b). The current level of the redox peaks under the 20% stretched condition was slightly higher than that under the non-stretched condition, whereas its value remained almost the same after cyclic stretching (Fig. 2d and e, respectively, original plot is shown in Figs. S7 and S8). The FE-SEM images of the working electrode before (left panel in Fig. 2f) and after (right panel in Fig. 2f) cyclic stretching show that only a few cracks were generated by the cyclic stretching experiment, and the structure of the 3D-nanostructured Au on the mogul-patterned substrate did not change significantly during the cyclic stretching. Therefore, our stretchable, three-electrode impedimetric biosensor with a Au 3D-nanostructured working electrode showed effective signal enhancement, good mechanical stability, and a minimal footprint, making it suitable for wearable cortisol detection.

3.4. Evaluation of label-free cortisol immunodetection performance

To detect the target biomolecule, cortisol, we used the electrochemical impedimetric spectroscopy (EIS) technique. To use faradaic EIS in our biosensor, we measured the electron transfer resistance (R_{et}) value, which corresponds to the radius of a semicircle in a Nyquist plot, in the redox mediator solution (10 mM $[K_3Fe(CN)_6]$ in 1X PBS). At the sensor level (without integration of the microfluidic device), the difference in the R_{et} before and after the affinity reaction between the probe Ab and antigen (Ag), $\Delta R_{et,sensor} = (R_{et,Ab-Ag}(S) - R_{et,Ab}(S))$, increased as the target concentration increased (Dong et al., 2013; Li et al., 2015; Liu et al., 2012). Here, $R_{et,\ Ab}(S)$ is the R_{et} value from the sensor with the probe Ab immobilized, and $R_{et,Ab-Ag}(S)$ is the R_{et} value from the sensor upon capturing target cortisol Ag molecules (Fig. S9).

So, $R_{et,\ Ab-Ag}(S)$ and $\Delta R_{et,sensor}$ increase with the target concentration because redox molecules find it difficult to reach the electrode surface when it is covered by conjugated Ab–Ag complexes. The $\Delta R_{et,sesnor}$ values obtained from the Nyquist plots with various cortisol concentrations showed a wide dynamic range, from 1 pg/ml to 1 μg/ ml, which encompasses the range of cortisol concentrations in sweat (Fig. 2g and Fig. S10) (Jang et al., 2018; Kaushik et al., 2014; Parlak et al., 2018).

The high surface-area of the Au 3D-nanostructured electrode creates a high density of immobilized Ab, which optimizes the sensing performance in terms of both sensitivity and dynamic range. The calibration curve for the biosensor with the Au 3D-nanostructured working electrode presented an LOD as low as 1 pg/ml, sensitivity of 0.25 Ohm/ng ml-1, and good linearity (Fig. 2h). On the other hand, the biosensor made with a Au thin-film working electrode on the mogul-patterned substrate had an initial impedance level larger than that of the Au 3D-nanostructured electrode and a smaller area for Ab immobilization (Fig. S11). Therefore, the change ratio in the electron transfer resistance ($\Delta R_{et,\ sesnor}/R_{et,Ab}(S)$) of the biosensor made with a Au thin-film electrode was smaller than that of the biosensor made with the Au 3D-nanostructured electrode over a cortisol concentration range of 1 pg/ml – 1 μg/ ml (Fig. 2i). For example, the $\Delta R_{et,\ sesnor}/R_{et,Ab}(S)$ of the biosensor with the Au thin-film electrode was 49.4%, whereas that of the biosensor with the Au 3D-nanostructured working electrode was 232.3% at a 1 $\mu g/\ ml$ cortisol concentration. Therefore, the 3D-nanostructuring of the working electrode played a critical role in enabling on-body immunodetection by enhancing the impedimetric signal enough to encompass the cortisol concentration range in human sweat.

The selectivity of label-free impedimetric biosensor for cortisol sensing should be tested against interference from molecules also present in sweat at similar solution conditions. In particular, neuropeptide Y (NPY) is present in human sweat and has a similar function to cortisol (Cizza et al., 2008). We calculated $R_{et,Ab-Ag}(S)$ values in the 10 mM $K_3[Fe(CN)_6]$ and PBS 1X solution after incubation with cortisol (1 ng/ml), NPY (1 ng/ml), cortisol (10 ng/ml), and NPY (10 ng/ml) in sequence. The $R_{et,Ab-Ag}(S)$ value from the Nyquist plots increased only when the sensor was incubated with the cortisol-spiked artificial sweat (Fig. S12). Thus, our biosensor shows good selectivity for cortisol against NPY.

To investigate the effect of mechanical deformation on our stretchable immunosensor, we conducted EIS measurements under stretched conditions of 10%, 20%, and 30% strain with a cortisol concentration with 1 ng/ml (Fig. 2j). The $R_{et,Ab-Ag}(S)$ values did not change significantly even under the 30% stretched condition because they are mainly affected by how many Ab and Ag molecules are conjugated on the surface. Because the mogul pattern on the stretchable PDMS substrate is flattened by stretching, the effective area of the working electrode is not expected to change significantly with stretching up to 30%. Therefore, our stretchable, label-free biosensor fabricated on the mogul-patterned substrate can be used for skin-mountable, quantitative immunodetection of cortisol in sweat.

3.5. Evaluation of integrated biosensor patch

To verify the performance of our integrated LOP containing both our microfluidic device and electrochemical biosensor, we conducted EIS

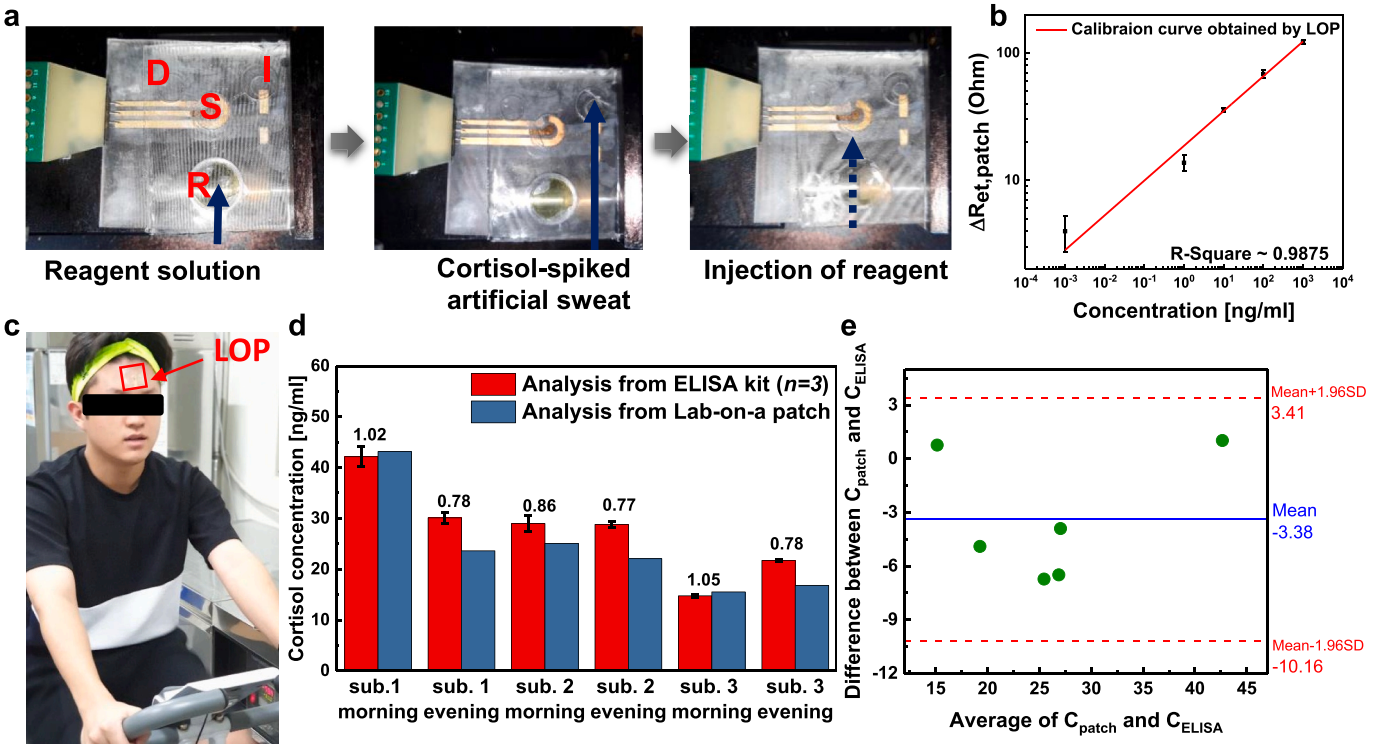

Fig. 3. Characterization of the integrated LOP platform (microfluidic device and biosensor patch) and demonstration of on-body immunodetection. (a) Picture of the LOP measuring the cortisol level in artificial sweat while loaded in a customized stretching rig connected to a potentiostat. The electrode lines of the working, counter, and reference electrodes are connected to bendable probe tips for measurement. The artificial sweat spiked with cortisol was dropped into the I. Then, after waiting for 15 min, the reagent solution was injected into the R by pushing the button, and the EIS curve was determined directly. **(b)** Calibration curve for the $\Delta R_{et,\ patch}$ obtained from the LOP as a function of cortisol concentration (results of triplicated experiments, *n=3*). **(c)** Picture of human subject 1, who exercised by cycling while the LOP was attached to their forehead. **(d)** Cortisol concentration results from an ELISA kit and the LOP assay for 6 samples, 2 each (one from the morning and one from the evening) from subjects 1, 2, and 3. The error bar is indicated on the analysis from the ELISA kit (n = 3), and the relative difference in the measured concentrations from the ELISA and LOP assays, ($|C_{ELISA} - C_{Patch}|/C_{ELISA}$), is marked above the bar graph **(e)** Comparison of the cortisol concentration analyses from the ELISA kit (C_{ELISA}) and LOP (C_{Patch}). The data are presented as Bland-Altman plot.

testing of cortisol in artificial sweat (ISO standard, pH 5.5) after integrating our microfluidic device with our stretchable impedimetric biosensor(Kulthong et al., 2010). First, however, we measured the $R_{et,Ab}(S)$ of the Ab-immobilized biosensor to calculate the ΔR_{et} value because the passive microfluidic device is disposable. After integration with the microfluidic device, 500 μL of the redox meditator solution was carefully injected into the R. When 100 μL of the artificial sweat spiked with cortisol was dropped on the I, it flowed passively to the S and filled it within 2 min. After the 15-min incubation, the R was activated by pushing the button, and the $R_{et,Ab-Ag}(P)$ value, which is the R_{et} value in the patch with Ab-Ag binding, was measured (Fig. 3a).

We prepared cortisol-spiked artificial sweat samples at various concentrations, 1 pg/ml, 1 ng/ml, 10 ng/ml, 100 ng/ml, *and* 1 $\mu g/$ ml, and calculated the $R_{et,\ Ab-Ag}(P)$ values from multiple biosensors upon target binding (Fig. S13) to determine $\Delta R_{et,patch} = (R_{et,\ Ab-Ag}(P) - R_{et,\ Ab}(S))$. We observed a shift compared with $\Delta R_{et,sesnor}$ and explained in Supplementary Information in detail (Fig. S14). The average value of $\Delta R_{et,\ patch}$ was obtained in triplicate at each concentration in the biosensor patch integrated with the microfluidic device, and the obtained calibration curve was fitted with the relation $\log(\Delta R_{et,\ patch}) = 0.27316 \times \log(concentration) + 1.27087$ in a detection range from 1 pg/ml to 1 μg/ml and a sensitivity of 0.273 Ohm/ng ml^{-1} (Fig. 3b).

3.6. On-body immunodetection of cortisol in sweat during exercise

To evaluate the biosensor patch integrated with the microfluidic device for on-body immunodetection in a real application, we attached it to the foreheads of three healthy human subjects and measured the cortisol levels in their sweat during exercise (Fig. 3c). The sweat cortisol levels were monitored twice in each subject: in the morning (9:00 a.m.) and evening (6:00 p.m.). The subjects exercised by cycling, and the sweat from their skin accumulated in the I and then passively flowed into the S. Generally, the sweat rate is reported to be 50–130 μl/cm^2/hr during exercise (Choi et al., 2018; Nyein et al., 2018, 2019). The area of the I is around 50.24 mm^2, so the S, with a volume of 27 μL, can be filled completely within 30–40 min after starting exercise even though the sweat rate differs from person to person. Once the S is full, sweat stops entering because of the bursting valve between the S and the D. In that way, the amount sweat is self-metered for precise target quantitation. During exercise, sweat samples from each subject were also collected in vials for a comparative analysis using a commercial ELISA kit. After the 15-min incubation in the S for the cortisol to bind with the Ab probes, the R button was pushed to inject the reagent solution into the S, and faradaic EIS was performed. The $R_{et,Ab-Ag}(P)$ value was calculated from the integrated patch and converted to cortisol concentration using a calibration curve (Fig. 3d). Subject 1 had the highest cortisol concentration among the subjects, and subject 3 had the lowest cortisol level. The tendency of increased cortisol in the morning and decreased cortisol in the evening was observed in subjects 1 and 2 but not in subject 3. Cortisol levels vary according to personal circadian cycles, generally increasing during the day and decreasing at night (Kaushik et al., 2014). Thus, personalized monitoring is needed to diagnose personal stress levels.

The concentrations of cortisol obtained from the microfluidics-integrated biosensor patch (C_{patch}) were compared with those measured by the cortisol ELISA assay (C_{ELISA}) (Table S2, Fig. 3d and 3e). The C_{ELISA} values (triplicated) were obtained using the four parameter logistics (4-PL) calibration curve (Fig. S15). We evaluated the relative accuracy of cortisol detection by comparing the biosensor patch results with the standard ELISA assay results ($|C_{ELISA} - C_{Patch}|/C_{ELISA}$). The average difference between the two assay results was about 14.7%, with a standard deviation of 9.38% (Table S3 and Fig. 3e). Even though the number of sweat samples for the two assays was small, the cortisol levels obtained from the LOP assay were similar to those in the ELISA assay.

4. Conclusions

No previous researchers had successfully integrated sample-controlling microfluidics and a skin-mountable biosensor into fully functional lab-on-a-chip technology. We met those challenges using the specifically designed valves and channels of our microfluidic device, which enables one-touch operation for simultaneous mediator delivery and washing. Using those techniques, we built an all-in-one, integrated microfluidics-electrochemical biosensor patch that provides wearable immunodetection of cortisol in human sweat. Our proposed LOP platform, which can complete all the steps required to detect low-concentration biomarkers, is very promising, especially if it can be combined with a wearable electrochemical reader with circuitry for impedance signal readout and wireless data transmission. Furthermore, wearable biosensor systems based on our LOP platform could be extended to detect other biomarkers in sweat (such as cytokines and neuropeptides), therapeutic drugs in sweat, and more diverse biomarkers in other biofluids, including interstitial fluids or wound exudate.

Declaration of competing interest

The authors declare that they have no known competing financial interests or personal relationships that could have appeared to influence the work reported in this paper.

CRediT authorship contribution statement

Han-Byeol Lee: Conceptualization, Methodology, Validation, Investigation, Writing - original draft. **Montri Meeseepong:** Methodology. **Tran Quang Trung:** Conceptualization, Methodology. **Bo-Yeong Kim:** Investigation. **Nae-Eung Lee:** Conceptualization, Writing - review & editing, Supervision.

Acknowledgements

This work was supported by the Basic Science Research Program (2019R1A6A1A03033215) and also by the Nano Material Technology Development Program (NRF-2016M3A7B4910554) through the National Research Foundation (NRF), funded by the Ministry of Science, ICT, & Future Planning.

Appendix A. Supplementary data

Supplementary data to this article can be found online at https://doi.org/10.1016/j.bios.2020.112133.

References

Alizadeh, A., Burns, A., Lenigk, R., Gettings, R., Ashe, J., Porter, A., McCaul, M., Barrett, R., Diamond, D., White, P., 2018. Lab Chip 18 (17), 2632–2641.
Andreu-Perez, J., Leff, D.R., Ip, H.M.D., Yang, G., 2015. IEEE Trans. Biomed. Eng. 62 (12), 2750–2762.
Bae, C.W., Toi, P.T., Kim, B.Y., Lee, W.I., Lee, H.B., Hanif, A., Lee, E.H., Lee, N.-E., 2019. ACS Appl. Mater. Interfaces 11 (16), 14567–14575.
Bandodkar, A.J., Jeang, W.J., Ghaffari, R., Rogers, J.A., 2019. Annu. Rev. Anal. Chem. 12 (1), 1–22.
Bandodkar, A.J., Jeerapan, I., Wang, J., 2016. ACS Sens. 1 (5), 464–482.
Bandodkar, A.J., Wang, J., 2014. Trends Biotechnol. 32 (7), 363–371.
Bariya, M., Nyein, H.Y.Y., Javey, A., 2018. Nat. Electron. 1 (3), 160–171.
Chen, X., Wang, Y., Zhou, J., Yan, W., Li, X., Zhu, J.-J., 2008. Anal. Chem. 80 (6), 2133–2140.
Chen, Z., Jiang, J., Shen, G., Yu, R., 2005. Anal. Chim. Acta 553 (1), 190–195.
Cho, H., Kim, H.-Y., Kang, J.Y., Kim, T.S., 2007. J. Colloid Interface Sci. 306 (2), 379–385.
Choi, J., Ghaffari, R., Baker, L.B., Rogers, J.A., 2018. Sci. Adv. 4 (2), eaar3921.
Choi, J., Xue, Y., Xia, W., Ray, T.R., Reeder, J.T., Bandodkar, A.J., Kang, D., Xu, S., Huang, Y., Rogers, J.A., 2017. Lab Chip 17 (15), 2572–2580.
Cizza, G., Marques, A.H., Eskandari, F., Christie, I.C., Torvik, S., Silverman, M.N., Phillips, T.M., Sternberg, E.M., Group, P.S., 2008. Biol. Psychiatr. 64 (10), 907–911.

Corrie, S.R., Coffey, J., Islam, J., Markey, K., Kendall, M., 2015. Analyst 140 (13), 4350–4364.
Daniels, J.S., Pourmand, N., 2007. Electroanal. Int. J. Fund. Pract. Asp. Electroanal. 19 (12), 1239–1257.
Dastider, S.G., Barizuddin, S., Dweik, M., Almasri, M., 2013. RSC Adv. 3 (48), 26297–26306.
Dong, J., Zhao, H., Xu, M., Ma, Q., Ai, S., 2013. Food Chem. 141 (3), 1980–1986.
Emaminejad, S., Gao, W., Wu, E., Davies, Z.A., Yin Yin Nyein, H., Challa, S., Ryan, S.P., Fahad, H.M., Chen, K., Shahpar, Z., Talebi, S., Milla, C., Javey, A., Davis, R.W., 2017. Proc. Natl. Acad. Sci. Unit. States Am. 114 (18), 4625–4630.
Gao, W., Emaminejad, S., Nyein, H.Y.Y., Challa, S., Chen, K., Peck, A., Fahad, H.M., Ota, H., Shiraki, H., Kiriya, D., 2016. Nature 529 (7587), 509–514.
Gao, W., Ota, H., Kiriya, D., Takei, K., Javey, A., 2019. Acc. Chem. Res. 52 (3), 523–533.
Glennon, T., O'Quigley, C., McCaul, M., Matzeu, G., Beirne, S., Wallace, G.G., Stroiescu, F., O'Mahoney, N., White, P., Diamond, D., 2016. Electroanalysis 28 (6), 1283–1289.
Gokaltun, A., Yarmush, M.L., Asatekin, A., Usta, O.B., 2017. Technology 5, 1–12, 01.
Guinovart, T., Valdés-Ramírez, G., Windmiller, J.R., Andrade, F.J., Wang, J., 2014. Electroanalysis 26 (6), 1345–1353.
Haji-Hashemi, H., Safarnejad, M.R., Norouzi, P., Ebrahimi, M., Shahmirzaie, M., Ganjali, M.R., 2019. Anal. Biochem. 566, 102–106.
Han, K.N., Li, C.A., Seong, G.H., 2013. Annu. Rev. Anal. Chem. 6, 119–141.
He, X., Xu, T., Gu, Z., Gao, W., Xu, L.-P., Pan, T., Zhang, X., 2019. Anal. Chem. 91 (7), 4296–4300.
Heikenfeld, J., Jajack, A., Rogers, J., Gutruf, P., Tian, L., Pan, T., Li, R., Khine, M., Kim, J., Wang, J., 2018. Lab Chip 18 (2), 217–248.
Huang, X., Liu, Y., Chen, K., Shin, W.J., Lu, C.J., Kong, G.W., Patnaik, D., Lee, S.H., Cortes, J.F., Rogers, J.A., 2014. Small 10 (15), 3083–3090.
Imani, S., Bandodkar, A.J., Mohan, A.M.V., Kumar, R., Yu, S., Wang, J., Mercier, P.P., 2016. Nat. Commun. 7 (1), 11650.
Jang, H.-J., Lee, T., Song, J., Russell, L., Li, H., Dailey, J., Searson, P.C., Katz, H.E., 2018. ACS Appl. Mater. Interfaces 10 (19), 16233–16237.
Jeerapan, I., Sempionatto, J.R., Pavinatto, A., You, J.-M., Wang, J., 2016. J. Mater. Chem. 4 (47), 18342–18353.
Jia, W., Bandodkar, A.J., Valdés-Ramírez, G., Windmiller, J.R., Yang, Z., Ramírez, J., Chan, G., Wang, J., 2013. Anal. Chem. 85 (14), 6553–6560.
Joung, H.-A., Ballard, Z.S., Ma, A., Tseng, D.K., Teshome, H., Burakowski, S., Garner, O. B., Di Carlo, D., Ozcan, A., 2019. Lab Chip 19 (6), 1027–1034.
Kallempudi, S.S., Altintas, Z., Niazi, J.H., Gurbuz, Y., 2012. Sensor. Actuator. B Chem. 163 (1), 194–201.
Kassal, P., Kim, J., Kumar, R., de Araujo, W.R., Steinberg, I.M., Steinberg, M.D., Wang, J., 2015. Electrochemistry 56, 6–10.
Kaushik, A., Vasudev, A., Arya, S.K., Pasha, S.K., Bhansali, S., 2014. Biosens. Bioelectron. 53, 499–512.
Kim, B.-Y., Lee, H.-B., Lee, N.-E., 2019a. Sensor. Actuator. B Chem. 283, 312–320.
Kim, J., Campbell, A.S., de Ávila, B.E.-F., Wang, J., 2019b. Nat. Biotechnol. 37, 389–406.
Kim, J., Sempionatto, J.R., Imani, S., Hartel, M.C., Barfidokht, A., Tang, G., Campbell, A. S., Mercier, P.P., Wang, J., 2018. Adv. Sci. 1800880.
Koh, A., Kang, D., Xue, Y., Lee, S., Pielak, R.M., Kim, J., Hwang, T., Min, S., Banks, A., Bastien, P., 2016. Sci. Transl. 366ra165.
Kokkinos, C., Economou, A., Prodromidis, M.I., 2016. Trac. Trends Anal. Chem. 79, 88–105.
Kulthong, K., Srisung, S., Boonpavanitchakul, K., Kangwansupamonkon, W., Maniratanachote, R., 2010. Part Fibre Toxicol. BioMed Central, 8-8.
Lee, E.K., Kim, M.K., Lee, C.H., 2019. Annu. Rev. Biomed. Eng. 21, 299–323.
Lee, H.-B., Bae, C.-W., Duy, L.T., Sohn, I.-Y., Kim, D.-I., Song, Y.-J., Kim, Y.-J., Lee, N.-E., 2016a. Adv. Mater. 28 (16), 3069–3077.
Lee, H., Choi, T.K., Lee, Y.B., Cho, H.R., Ghaffari, R., Wang, L., Choi, H.J., Chung, T.D., Lu, N., Hyeon, T., Choi, S.H., Kim, D.-H., 2016b. Nat. Nanotechol. 11, 566–572.
Li, Z., Fu, Y., Fang, W., Li, Y., 2015. Sensors 15 (8), 19212–19224.
Liu, G., Iyengar, S.G., Gooding, J.J., 2012. Electroanalysis 24 (7), 1509–1516.
Martín, A., Kim, J., Kurniawan, J.F., Sempionatto, J.R., Moreto, J.R., Tang, G., Campbell, A.S., Shin, A., Lee, M.Y., Liu, X., Wang, J., 2017. ACS Sens. 2 (12), 1860–1868.
Matzeu, G., Florea, L., Diamond, D., 2015. Sensor. Actuator. B Chem. 211, 403–418.
Meng, L., Turner, A.P., Mak, W.C., 2019. Biotechnol. Adv.
Nyein, H.Y.Y., Bariya, M., Kivimäki, L., Uusitalo, S., Liaw, T.S., Jansson, E., Ahn, C.H., Hangasky, J.A., Zhao, J., Lin, Y., Happonen, T., Chao, M., Liedert, C., Zhao, Y., Tai, L.-C., Hiltunen, J., Javey, A., 2019. Sci. Adv. eaaw9906.
Nyein, H.Y.Y., Tai, L.-C., Ngo, Q.P., Chao, M., Zhang, G.B., Gao, W., Bariya, M., Bullock, J., Kim, H., Fahad, H.M., 2018. ACS Sens. 3 (5), 944–952.
Oh, K.W., Lee, K., Ahn, B., Furlani, E.P., 2012. Lab Chip 12 (3), 515–545.
Panneer Selvam, A., Muthukumar, S., Kamakoti, V., Prasad, S., 2016. Sci. Rep. 23111.
Parlak, O., Keene, S.T., Marais, A., Curto, V.F., Salleo, A., 2018. Sci. Adv. eaar2904.
Pingarron, J.M., Yanez-Sedeno, P., Gonzalez-Cortes, A., 2008. Electrochim. Acta 53 (19), 5848–5866.
Ramasamy, S.K., 2017. Stem Cells Int., p. 5046953.
Ray, T.R., Choi, J., Bandodkar, A.J., Krishnan, S., Gutruf, P., Tian, L., Ghaffari, R., Rogers, J.A., 2019. Chem. Rev. 119 (8), 5461–5533.
Reeder, J.T., Choi, J., Xue, Y., Gutruf, P., Hanson, J., Liu, M., Ray, T., Bandodkar, A.J., Avila, R., Xia, W., Krishnan, S., Xu, S., Barnes, K., Pahnke, M., Ghaffari, R., Huang, Y., Rogers, J.A., 2019. Sci. Adv., eaau6356
Salvo, P., Dini, V., Di Francesco, F., Romanelli, M., 2015. Wound Med. 8, 15–18.
Someya, T., Amagai, M., 2019. Nat. Biotechnol. 37 (4), 382–388.
Steckl, A.J., Ray, P., 2018. ACS Sens. 3 (10), 2025–2044.
Stone, H.A., Stroock, A.D., Ajdari, A., 2004. Annu. Rev. Fluid Mech. 36, 381–411.
Tamayol, A., Akbari, M., Zilberman, Y., Comotto, M., Lesha, E., Serex, L., Bagherifard, S., Chen, Y., Fu, G., Ameri, S.K., Ruan, W., Miller, E.L., Dokmeci, M.R., Sonkusale, S., Khademhosseini, A., 2016. Adv. Healthc. Mater. 5 (6), 711–719.
Toi, P.T., Trung, T.Q., Dang, T.M.L., Bae, C.W., Lee, N.-E., 2019. ACS Appl. Mater. Interfaces 11 (11), 10707–10717.
Tomazelli Coltro, W.K., Cheng, C.M., Carrilho, E., de Jesus, D.P., 2014. Electrophoresis 35 (16), 2309–2324.
Trung, T.Q., Lee, N.-E., 2016. Adv. Mater. 28 (22), 4338–4372.
Windmiller, J.R., Wang, J., 2013. Electroanalysis 25 (1), 29–46.
Xu, G., Cheng, C., Liu, Z., Yuan, W., Wu, X., Lu, Y., Low, S.S., Liu, J., Zhu, L., Ji, D., 2019a. Adv. Mat. Technol. 1800658.
Xu, S., Jayaraman, A., Rogers, J.A., 2019b. Nature 571, 319–321.
Zamora, M., Dominguez, J., Trujillo, R., Goy, C., Sánchez, M., Madrid, R., 2018. Sensor. Actuator. B Chem. 260, 601–608.
Zhao, J., Guo, H., Li, J., Bandodkar, A.J., Rogers, J.A., 2019. Trends Chem. 1 (6), 559–571.
Zhong, J., Zhang, Y., Zhong, Q., Hu, Q., Hu, B., Wang, Z.L., Zhou, J., 2014. ACS Nano 8 (6), 6273–6280.